Small-scale Physical Modelling of Geotextile-Reinforced Sand Fill over Hong Kong Marine Clay Improved by Deep Cement Mixed Soil Columns

P.C. Wu, Q. W. Xie, W.J. Zhao & J.H. Yin
The Hong Kong Polytechnic University, Hong Kong

doi: https://doi.org/10.21467/proceedings.7.7.5

ABSTRACT

Deep cement mixing (DCM) technology was introduced in Hong Kong for the first time in the reclamation project of the Third Runway System of the Hong Kong International Airport and has been used in many other projects afterwards to improve the soft marine clay. Load transfer platforms (LTP) with or without geotextile reinforcement are often designed to facilitate the load transfer from the reclamation fills to the seabed. In this study, a small-scale physical model test was conducted on a geotextile-reinforced sand fill over Hong Kong Marine Clay (HKMC) improved by DCM columns, aiming to investigate the load transfer mechanism among DCM, HKMD, and geotextile reinforcement. The load transfer mechanism was examined by looking into the vertical stresses measured by earth pressure cells at different locations. The mobilised tensile strain in the geotextile reinforcement was measured using Fibre Bragg Grating sensors. Efficacy was calculated to assess the performances of DCM on load transfer. Furthermore, commonly used design guidelines were reviewed and applied to determine the load taken by DCM and the maximum tensile strain of geotextile reinforcement. It was found that the results offered by Dutch and FHWA methods agreed well with the experimental data.

1 INTRODUCTION

The third runway reclamation project of the Hong Kong International Airport was constructed over a seabed of soft marine clay improved by deep cement mixing (DCM) method. Since then, DCM works have been applied in many other projects involving soft marine clay in Hong Kong. Load transfer platforms (LTP) with or without geosynthetic reinforcement are often designed to facilitate the load transfer from the reclamation fills to the seabed (Lee, 2016). The consideration of the load transfer mechanism and the design of geosynthetic reinforcements in LTP are similar to geosynthetic-reinforced column-supported (GRCS) embankments. The load transfer is normally related to soil arching effect which develops with the settlement of subsoils or the deflection of geosynthetic reinforcements (Iglesia et al., 2014; King et al., 2017; Zhang et al., 2022; Wu et al., 2020 and 2024). Various theories and models for soil arching in column-supported embankments were proposed based on empirical methods or analytical approaches, among which the semi-spherical arches model proposed by Hewlett (1988), multi-shell arches model proposed by Zaesek (2001), and concentric arches (CA) model proposed by van Eekelen et al. (2013) have been adopted in British, German, and Dutch design guidelines. Adopting different design guidelines leads to different considerations of arching effect and predictions of tensile strain in the reinforcement, hence affecting the design and selection of geosynthetic reinforcement.

In this study, a small-scale physical model test was conducted on a geotextile-reinforced sand fill over Hong Kong Marine Clay (HKMC) improved by DCM columns, aiming to investigate the load transfer mechanism among DCM, HKMC, and geotextile reinforcement. The load transfer mechanism was examined by looking into the vertical stresses measured by earth pressure cells at different locations. The mobilised tensile strain in the geotextile reinforcement was measured using Fibre Bragg Grating sensors. Efficacy was

Proceedings DOI: 10.21467/proceedings.7.7; Series: AIJR Proceedings; ISSN: 2582-3922; ISBN: 978-81-989164-3-3

calculated to assess the performances of DCM on load transfer. The experimental results were then compared with the predictions according to current design guidelines, such as British standard BS8006, German design recommendation, Dutch CUR design method, and American FHWA design manuals.

2 Experiment setup

2.1 Experiment setup, materials and instrumentation

A small-scale physical model test was conducted in a steel tank with dimensions of 1000 mm (length) × 600 mm (width) × 800 mm (depth), as shown in Figure. 1. Six DCM columns were installed in the subsoil of Hong Kong Marine Clay (HKMC). A geotextile-reinforced sand layer was placed over the DCM-improved HKMC.

Reconstituted HKMC used in this physical model was originally excavated from coastal area of Lantau Island in Hong Kong. HKMC is of high compressibility and notable plasticity. The basics properties of HKMC and sand were listed in Table 1. DCM columns (100 mm in diameter, 400 mm in length) were prepared by mixing ordinary Portland cement with HKMC with the water content of 100%. Cement content (dry mass of cement to dry mass of HKMC) was 20%. Unconfined compressive strength q_u and secant Young's modulus E_{50} were around 0.6 MPa and 70 MPa, respectively, after 28-day curing. A woven geotextile with secant tensile modulus J of 680 kN/m in the longitudinal direction and 150 kN/m in the transversal direction were used as a reinforcement.

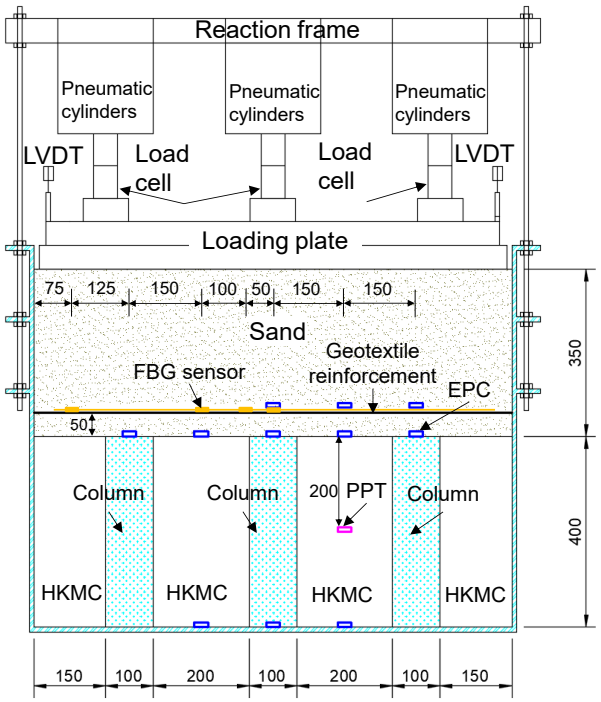

Figure 1: Physical model setup

Table 1: Basic properties of HKMC and sand

Soil	Property	Value
HKMC	G_s	2.65
	LL (%)	43.2
	PL (%)	22.6
	PI (%)	20.6
	w_0 (%)	100
	CR	0.24
	RR	0.03
Sand	G_s	2.56
	$\rho_{d,max}$ (Mg/m^3)	1.742
	$\rho_{d,min}$ (Mg/m^3)	1.536
	w_{opt} (%)	16.5

Proceedings DOI: 10.21467/proceedings.7.7
ISBN: 978-81-989164-3-3

Series: AIJR Proceedings
ISSN: 2582-3922

	φ'	34.6

Earth pressure cells (EPCs) were installed at different locations to measure the vertical stresses. One pore pressure transducer (PPT) was placed at the bottom and one was placed at the middle level of the subsoils to monitor the changes in excess pore pressure. Linear variable differential transformers (LVDTs) were used to measure the surface settlement. Surcharge load was applied using a self-designed loading system consisting of six pneumatic cylinders. The actual loading output of the loading system was monitored by load cells. Fibre Bragg grating (FBG) sensors were adopted to measure the tensile strength of the geotextile reinforcement. Each FBG sensor covered a sensing zone with a length of 100 mm, with the measured strain from the sensor representing the average strain within the sensing zone.

2.2 Testing program

A multi-stage loading test was performed using the self-designed loading system following a loading sequence of 10, 20, and 40 kPa. Surface settlements were measured during the loading tests. Each loading was conducted until the excess pore pressure was nearly fully dissipated. Figure 2 shows the measured surface settlement and excess pore pressures during the loading test.

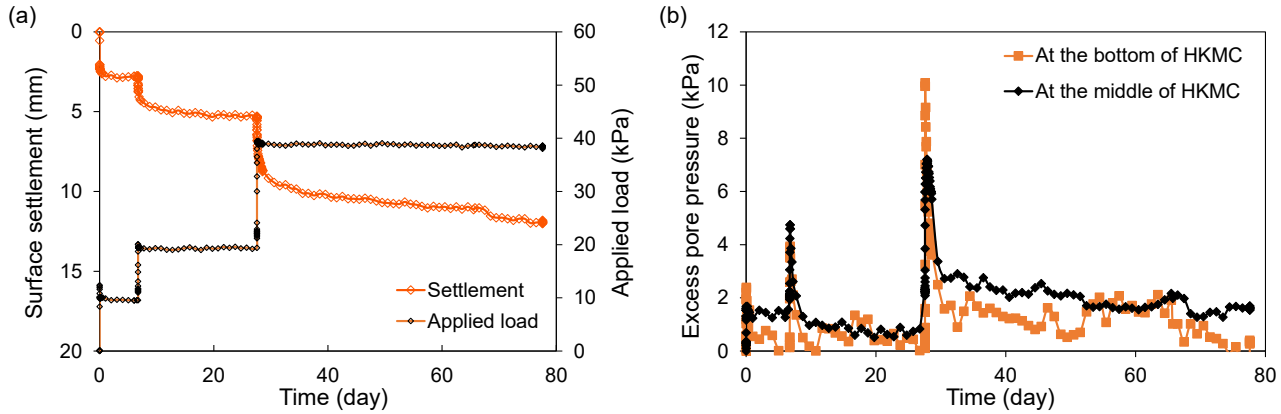

Figure 2: (a) Measured surface settlement and applied load and (b) measured excess pore pressures

3 Experiment results

3.1 Vertical stress and load distribution

To better address the mechanism of load transfer, the model test is divided into three zones, namely column, strip, and square zones, as shown in Figure 3(a). The column zone covers the DCM columns and the portion of the sand layer above the columns, the strip zone is the area between two adjacent column zones, and the square zone is the area enclosed by four strip zones. Strip and square zones are similar to those adopted by van Eekelen et al. (2015). It should be noted that the difference between vertical stresses above and beneath the geotextile in the column zone may be significant, depending on the development of the membrane effect of the geotextile. The circular cross section of columns can be converted into a square with an equivalent size of a. The area influenced by each column is illustrated using a column-soil unit, as shown in Figure 3(b).

The load transfer can be divided into load parts A, B, and C, which are the portions of the load acting on columns, transferred to geotextile, and supported by the HKMC subsoil, respectively, as illustrated in Figure 3(c). In this study, the vertical stresses above and beneath the geotextile in the column zone were used to calculate load parts A and $A + B$, respectively, whereas those beneath the geotextile in the strip and square zones were used to determine load part C. The equations for determining load parts A, B, and C are provided as follows.

$$A = \sigma_c^a A_c \tag{1}$$

$$B = \left(\sigma_c^b - \sigma_c^a\right) A_c \tag{2}$$

$$C = \sigma^b_{strip} A_{strip} + \sigma^b_{square} A_{squre} \tag{3}$$

where σ^a_c and σ^b_c are the vertical stresses above and beneath the geotextile in the column zone, respectively, σ^b_{strip} represents the vertical stress beneath the geotextile in the strip zone, σ^b_{square} is the vertical stress beneath the geotextile in the square zones, and A_c, A_{strip}, and A_{square} are the areas of the column, strip , and square zones within each column-soil unit, respectively. σ^a_{strip} and σ^a_{square} are the vertical stresses above the geotextile in the strip and square zones, respectively. σ^a_c, σ^b_c, σ^b_{strip}, σ^b_{square}, σ^a_{strip}, σ^a_{square}, A_c, A_{strip}, and A_{square} are illustrated in Figure 6.

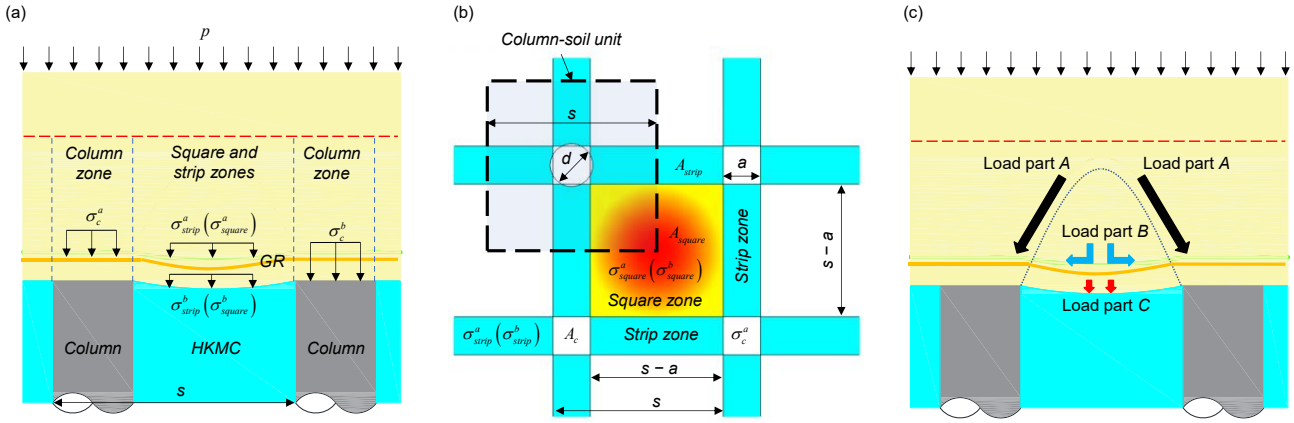

Figure 3: Illustrations of (a) column, square, and strip zones, (b) column-soil unit, and (c) load parts *A*, *B*, and *C*

Figure 4 shows load parts *A*, *B*, and *C* (per column-soil unit) calculated using the vertical stresses measured at different locations and time points. In the first loading stage, there was no significant difference between load parts *A* and *C*, and load part *B* was nearly zero, indicating a slight effect of the geotextile. As the surcharge load increased, load part *A* became the largest portion among the three load parts. A significant reduction occurred in the load taken by the HKMC subsoil. The increase in load part *B* indicated that the geotextile started to contribute to the load redistribution.

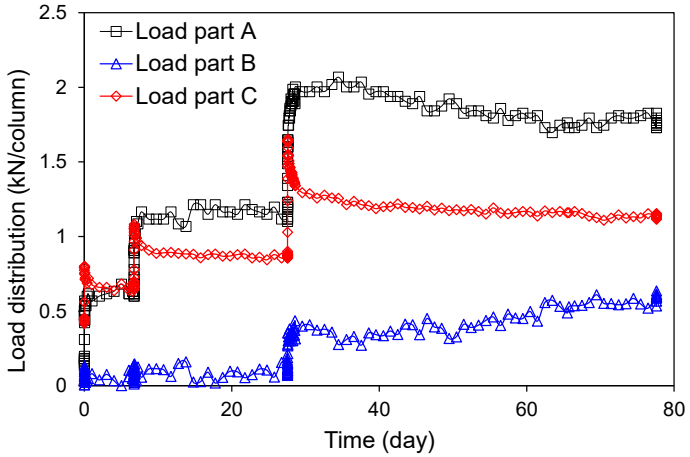

Figure 4: Load distribution in a column-soil unit regarding load parts *A*, *B*, and *C*

3.2 Tensile strain

Tensile strains of the geotextile reinforcement were measured by FBG sensors. The sensing principle of FBG can be expressed by the following equation:

Proceedings DOI: 10.21467/proceedings.7.7
ISBN: 978-81-989164-3-3

Series: AIJR Proceedings
ISSN: 2582-3922

$$\Delta\lambda_B / \lambda_{B0} = c_\varepsilon \Delta\varepsilon + c_T \Delta T \quad (4)$$

where λ_{B0} is the original Bragg wavelength, c_ε and c_T are the coefficients of strain and temperature, respectively. The wavelength change $\Delta\lambda_B$ is sensitive to strain and temperature. By detecting the wavelength changes, changes in strain or temperature can be determined. Figure 5 shows the calibration results between the wavelength change of FBG sensors and global strain of a geotextile with the testing range of 100 mm. It should be noted that the calibration tests and physical model test were performed under the constant temperature. Therefore, the temperature effect on wavelength change of FBG sensors was negligible in this study.

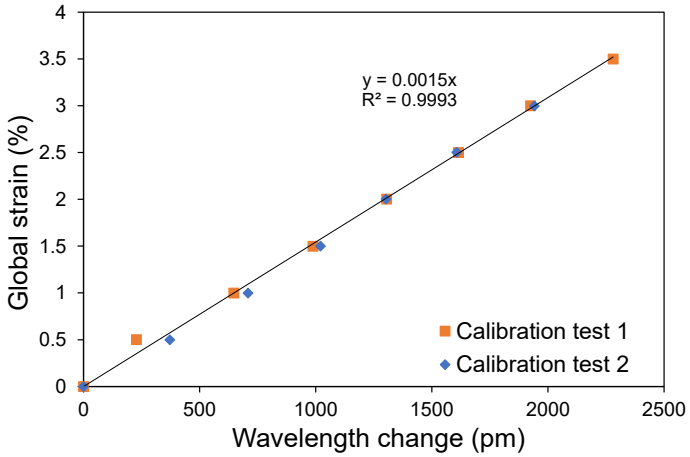

Figure 5: Calibration results of FBG sensors on geotextile

Figure 6 presents the measured maximum strains along the x direction (longitudinal) and y direction (transversal) of the geotextile. It can be seen that the strains in the y direction were greater than those in the x direction, owing to the greater stiffness of the geotextile in the x direction. The strains in both directions saw a significant increase as the surcharge loading reached 40 kPa, indicating that the geotextile started to contribute to the load redistribution. The development of tensile strains agreed reasonably with the load distribution curves presented in Figure 4.

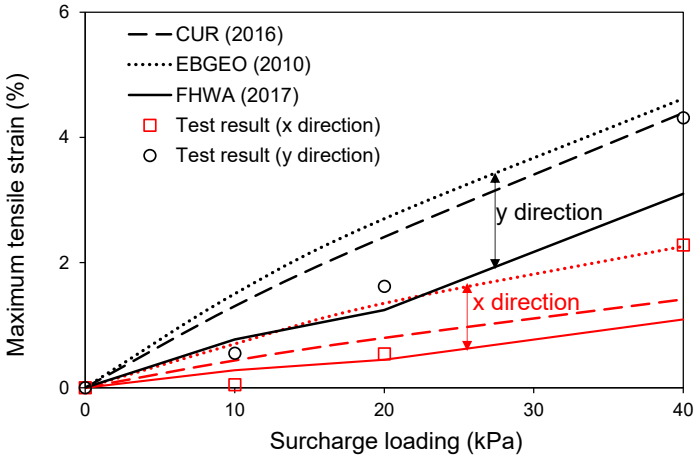

Figure 6: Maximum tensile strains

4 Discussion

4.1 Assessment of arching effect using current design method

In many design guidelines, arching effect can quantify by Efficacy, an index representing the proportion of the load taken by columns, which can be expressed by the following equation:

$$E = A \Big/ \left[\left(\gamma H + p \right) s^2 \right] \tag{5}$$

where p is the surcharge loading, s is the size of the column-soil unit, as indicated in Figure 3(b), γ and H are the unit weight and height of the sand fill, respectively.

The value of Efficacy is in the range of 0 to 1, with the greater value corresponding to greater arching effect. The development of Efficacy with surcharge loading of the small-scale physical model test is plotted in Figure 7.

It was found that Efficacy showed a decrease during the process of increasing the surcharge load. This was attributed to the partially undrained condition of the HKMC subsoil, which delayed the load transfer. The differential settlements between the columns and surrounding soil increased with the consolidation of the subsoil, resulting in an increase in the deflection of the reinforcement, and thus increasing the Efficacy. The Efficacy at the end of the consolidation slightly increased with an increase in surcharge load. A simplified pattern of the development of Efficacy with surcharge loading is also illustrated in Figure 7.

In this study, we reviewed and selected four widely used design guidelines and assessed them with the experimental data of the small-scale physical model test. Those design guidelines are (1) British BS 8006 guidelines, (2) German EBGEO guidelines, (3) American FHWA manuals, and (4) Dutch CUR guidelines. The main theories adopted in this design guidelines are summarised in Table 2.

Table 2: A summary of different design guidelines

Design guidelines	Theories/methods	Remarks
BS8006 guidelines	Hewlett and Randolph (1998) method – Semi-spherical Arching model	A limit-state equilibrium model Ignore the subsoil support Apply to a square arrangement of columns Uniform loading distribution on reinforcements
German EBGEO guidelines	Multi-shell Arches model proposed by Zaeske (2001)	A limit-state equilibrium model The contribution of consolidation of subsoils to arching effect is not considered Consider subsoil support only when calculating tension of reinforcements Apply to a square arrangement of columns/piles. Triangular loading distribution on reinforcements
FHWA manuals	Adapted Terzaghi method (Sloan et al., 2011)	A friction model The results highly depend on the value of K_T (0.5-1). 0.75 is recommended. Can consider multiple layers of fill materials Consider subsoil support and consolidation of subsoil by using load-displacement compatibility (LDC) method (Filz et al., 2019) Uniform loading distribution on reinforcements
Dutch CUR guidelines	Concentric Arches (CA) model (van Eekelen, 2015)	A limit-state equilibrium model Apply to a square arrangement of columns Distinguish square and strip zones Uniform/inversed triangular loading distribution on reinforcements

In BS8006 design guidelines, Hewlett and Randolph's method was adopted to quantify the soil arching effect. German EBGEO adopted the multi-shell arches theory of Zaeske (2001). Adapted Terzaghi model was used in FHWA manuals. A three-dimensional concentric arches (CA) model developed by van Eekelen (2015) was adopted in Dutch CUR guidelines. The main equations used in different guidelines for determining Efficacy were listed in Wu et al. (2024).

Proceedings DOI: 10.21467/proceedings.7.7

Series: AIJR Proceedings
ISBN: 978-81-989164-3-3
ISSN: 2582-3922

Figure 7 presents the Efficacy values determined according to different design guidelines. Generally speaking, EBGEO (2010), CUR (2016) and FHWA (2017) gave Efficacy values similar to those calculated using experimental data. While the BS8006 (2010) overestimated the Efficacy by around 12 %. What leads to different results for various design guidelines is that actual deformations occurring in subsoil or reinforcement are incompatible with the required ones to achieve the arching state assumed by those guidelines.

Among the four design guidelines, the result of the FHWA (2017) agreed well with the trend of Efficacy calculated using the measured data. However, it should be noted that the results calculated by the adapted Terzaghi method are highly dependent on the value of K_T. Higher K_T values result in higher efficacies. Therefore, this method must be used with caution. The Efficacy values calculated according to BS8006 (2010), EBGEO (2010), and CUR (2016) remained constant under the different surcharge loads. This was because these methods are based on limit state equilibrium, which can only determine a constant arching stress value.

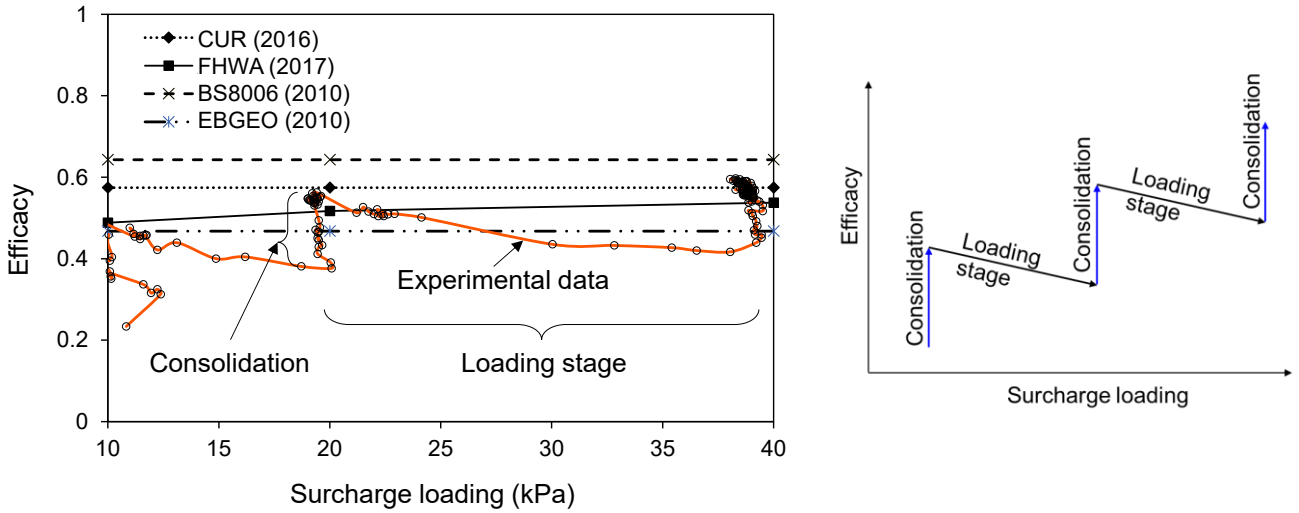

Figure 7: Development of efficacy with surcharge loading

4.2 Tensile strain

Since EBGEO (2010), CUR (2016), and FHWA (2017) provided better results in term of Efficacy, those three design guidelines were selected to further calculate the maximum tensile strains of the geotextile in the physical model.

In EBGEO (2010), design charts were provided to determine the maximum tensile strains of geosynthetic reinforcement. The equations used in Dutch design guidelines for calculating the maximum tensile strains can be referred to CUR (2016). In FHWA (2017), generalised parabolic method was adopted to determine the tension in biaxial geosynthetics placed in alignment with a rectangular array of column:

$$6T^3 + 6T\left(\frac{\sigma_{net}s^2}{p_c}\right)^2 - J\left(\frac{\sigma_{net}s^2}{p_c}\right) = 0 \tag{6}$$

where T is the tension in the geotextile, σ_{net} is the net vertical stress acting on the geotextile, p_c is the perimeter of the column, and J is the stiffness of the geotextile. The maximum tension of the geotextile can be determined by solving Equation (6), and therefore the tensile strain can be calculated as $\varepsilon=T/J$. Figure 6 presents the maximum tensile strains determined according to German, Dutch, and US design guidelines. It can be seen that Dutch CUR (2016) and US FHWA (2017) can predict the maximum tensile strains with reasonable agreement to the experimental data.

5 CONCLUSIONS

A small-scale physical model test on geotextile-reinforced sand layer over HKMC improved by DCM columns has been successfully conducted with the measurement of earth pressures and the tensile strains of the geotextile reinforcement. The load distribution was revealed based on the earth pressure data. It was found that during the loading stage, Efficacy of DCM columns decreased attributed to the partially undrained behaviour of HKMC. As the HKMC consolidated, load was transferred gradually to the column resulting in an increase in Efficacy. Furthermore, the predictions of Dutch design guidelines and FHWA manuals agreed reasonably with the experimental data in terms of Efficacy of DCM columns and the maximum tensile strains of the geotextile.

ACKNOWLEDGEMENTS

The work in this paper is supported by a General Research Fund (GRF) projects (15226722) from Research Grants Council (RGC) of Hong Kong Special Administrative Region Government of China. The authors also acknowledge the financial support from the Start-up fund (BD30) and two research grants from Research Institute for Land and Space (CD82 and CD7A) of The Hong Kong Polytechnic University.

REFERENCES

BS 8006 2010. Code of Practice for Strengthened/Reinforced Soils and Other Fills. British Standard Institution, UK

EBGEO 2010. Empfehlungen für den Entwurf und die Berechnung von Erdkörpern mit Bewehrungen aus Geokunststoffen e EBGEO, vol. 2 German Geotechnical Society, Auflage978-3-433-02950-3 (in German). Also available in English: Recommendations for Design and Analysis of Earth Structures using Geosynthetic Reinforcements e EBGEO, 2011. ISBN: 978-3-433-02983-1 and digital in English ISBN: 978-3-433-60093-1.

Filz, G. M., Sloan, J. A., McGuire, M. P., Smith, M., & Collin, J. (2019). Settlement and vertical load transfer in column-supported embankments. Journal of Geotechnical and Geoenvironmental Engineering, 145(10), 04019083.

Hewlett, W. J. 1988. Analysis of piled embankment. *Ground Engineering*. 21(3): 12-18.

Iglesia, G.R., Einstein, H.H., & Whitman, R.V. 2014. Investigation of soil arching with centrifuge tests. *Journal of Geotechnical and Geoenvironmental Engineering*, 140(2): 04013005.

King, D.J., Bouazza, A., Gniel, J.R., Rowe, R.K., & Bui, H.H. 2017. Load-transfer platform behaviour in embankments supported on semi-rigid columns: implications of the ground reaction curve. *Canadian Geotechnical Journal*, 54(8): 1158-1175.

Lee, D. 2016. Expansion of Hong Kong International Airport into a Three-Runway System, Airport Reclamations – then and now. HKIE YMC Seminar. http://ymc.hkie.org.hk/DocDown.aspx?imgDoc=151_160120+3RS+Reclamation+(20+Jan+2016).pdf

Schaefer, V. R., Berg, R. R., Collin, J. G., Christopher, B. R., DiMaggio, J. A., Filz, G. M., ... & Ayala, D. (2017). Ground modification methods reference manual—Volume II. Washington, DC: Federal Highway Administration.

Sloan, J., Filz, G., & Collin, J. (2011). A generalized formulation of the adapted Terzaghi method of arching in column-supported embankments. In Geo-Frontiers 2011: Advances in Geotechnical Engineering (pp. 798-805).

van Eekelen, S.J.M., Bezuijen, A., & Van Tol, A.F. 2013. An analytical model for arching in piled em-bankments. *Geotextiles and Geomembranes*, 39: 78-102.

van Eekelen, S. J. M. 2015. Basal reinforced piled embankments: Experiments, field studies and the development and validation of a new analytical design model.

CUR. 2016. Design guideline basal reinforced piled embankments. CRC press.

Wu, P. C., Feng, W. Q., & Yin, J. H. 2020. Numerical study of creep effects on settlements and load trans-fer mechanisms of soft soil improved by deep cement mixed soil columns under embankment load. *Geotextiles and Geomembranes*, 48(3): 331-348.

Wu, P. C., Chen, W. B., Feng, W. Q., Yin, J. H., Ho, T. O., & Huang, S. R. (2024). Load transfer mechanism of geotextile-reinforced sand layer over semirigid column-improved soft soil. *Acta Geotechnica*, 19(5), 2855-2871.

Zaeske, D. 2001. Zur Wirkungsweise von unbewehrten und bewehrten mineralischen Tragschichten über pfahlartigen Gründungselementen. Fachgebiet u. Versuchsanst. Geotechnik, Univ. Gh Kassel.

Zhang, C., Su, L., & Jiang, G. 2022. Full-scale model tests of load transfer in geogrid-reinforced and float-ing pile-supported embankments. *Geotextiles and Geomembranes*, 50(5):896-909.